UC Davis
UC Davis Previously Published Works

Title

β-Cell Succinate Dehydrogenase Deficiency Triggers Metabolic Dysfunction and Insulinopenic Diabetes

Permalink

https://escholarship.org/uc/item/71r94771

Journal

Diabetes, 71(7)

ISSN

0012-1797

Authors

Lee, Sooyeon
Xu, Haixia
Van Vleck, Aidan
et al.

Publication Date

2022-07-01

DOI

10.2337/db21-0834

Peer reviewed

β-Cell Succinate Dehydrogenase Deficiency Triggers Metabolic Dysfunction and Insulinopenic Diabetes

Sooyeon Lee,[1] Haixia Xu,[1] Aidan Van Vleck,[1] Alex M. Mawla,[2] Albert Mao Li,[3,4] Jiangbin Ye,[3,4] Mark O. Huising,[2,5] and Justin P. Annes[1,6]

Mitochondrial dysfunction plays a central role in type 2 diabetes (T2D); however, the pathogenic mechanisms in pancreatic β-cells are incompletely elucidated. Succinate dehydrogenase (SDH) is a key mitochondrial enzyme with dual functions in the tricarboxylic acid cycle and electron transport chain. Using samples from human with diabetes and a mouse model of β-cell–specific SDH ablation (SDHB^βKO), we define SDH deficiency as a driver of mitochondrial dysfunction in β-cell failure and insulinopenic diabetes. β-Cell SDH deficiency impairs glucose-induced respiratory oxidative phosphorylation and mitochondrial membrane potential collapse, thereby compromising glucose-stimulated ATP production, insulin secretion, and β-cell growth. Mechanistically, metabolomic and transcriptomic studies reveal that the loss of SDH causes excess succinate accumulation, which inappropriately activates mammalian target of rapamycin (mTOR) complex 1–regulated metabolic anabolism, including increased SREBP-regulated lipid synthesis. These alterations, which mirror diabetes-associated human β-cell dysfunction, are partially reversed by acute mTOR inhibition with rapamycin. We propose SDH deficiency as a contributing mechanism to the progressive β-cell failure of diabetes and identify mTOR complex 1 inhibition as a potential mitigation strategy.

Type 2 diabetes (T2D) is a chronic disease of altered glucose homeostasis, characterized by a progressive decrease in β-cell function and mass, also termed β-cell failure (1–3). Emerging evidence implicates mitochondrial dysfunction as a central contributor to β-cell failure and T2D pathogenesis (4–6); however, the pathophysiological mechanisms of β-cell mitochondrial dysfunction remain to be established. In β-cells, mitochondria play a fundamental role in coupling glucose metabolism to insulin secretion, ensuring strict regulation of glucose-stimulated insulin secretion (GSIS) and compensatory β-cell mass expansion (7). While the pivotal role of the mitochondria in coupling glucose metabolism to insulin secretion is well-characterized, less is known about the molecular mechanisms that link mitochondrial dysfunction to progressive β-cell dysfunction.

Succinate dehydrogenase (SDH), or complex II (CII), is one of five mitochondrial complexes that participates in the electron transport chain (ETC). SDH is composed of nuclear-encoded subunits (SDHA–D) that form a hetero tetrameric complex in the inner mitochondrial membrane (8). SDH also functions in the tricarboxylic acid (TCA) cycle by catalyzing the oxidation of succinate to fumarate (9). This enzymatic reaction is accompanied by the generation of $FADH_2$, which donates electrons to ubiquinone via CII for oxidative phosphorylation (9). The dual role of SDH in the ETC and TCA cycle places it at the nexus of mitochondrial metabolism and ATP generation. Accordingly, impaired SDH/CII activity is linked to severe human metabolic disorders, including Leigh syndrome and cardiomyopathy (reviewed in Refs. 10,11). Notably, the SDH complex is not required for oxidative phosphorylation as it can be bypassed through alternative metabolic pathways (11).

[1]Division of Endocrinology, Department of Medicine, Stanford University, Stanford, CA

[2]Department of Neurobiology, Physiology and Behavior, College of Biological Sciences, University of California, Davis, Davis, CA

[3]Department of Radiation Oncology, Stanford University School of Medicine, Stanford, CA

[4]Cancer Biology Program, Stanford University School of Medicine, Stanford, CA

[5]Department of Physiology and Membrane Biology, School of Medicine, University of California, Davis, Davis, CA

[6]Stanford ChEM-H and Diabetes Research Center, Stanford University School of Medicine, Stanford, CA

Corresponding author: Justin P. Annes, jannes@stanford.edu

Consequently, it is not fully understood how the loss of SDH profoundly impairs mitochondrial function. Proposed disease-causing consequences of SDH disruption are the intracellular accumulation of succinate, increased reactive oxygen species production, and impaired ATP generation (10–12).

SDH deficiency most severely impacts metabolically active cells with continuous energy requirements, such as cardiomyocytes, skeletal muscle cells, and neural cells (10,11); hence, β-cells, a highly metabolic cell type that functionally reports circulating glucose levels via ATP generation and insulin release, is an ideal cell type to investigate the biological function of SDH. Recent studies in rodent islets revealed that SDH/CII inhibition with 3-nitroprorionic acid impaired insulin secretion (13,14), uncovering a role for SDH in regulating β-cell function. Indeed, Wojtovich et al. (15) suggested that reduced SDH activity and consequent succinate accumulation might be causally linked to diabetes. In this study, we test the hypothesis that SDH deficiency is a driver of mitochondrial dysfunction in β-cell failure and diabetes pathogenesis.

RESEARCH DESIGN AND METHODS

Human Pancreas
All human pancreatic sections from age-, sex-, and BMI-matched healthy donors without diabetes (ND) and donors with T2D were obtained from the Network for Pancreatic Organ Donors with Diabetes (nPOD). Donor information is presented in Supplementary Table 1.

Animal Models
Animal experiments were performed in compliance with the Institutional Animal Care and Use Committee and the Stanford University Administrative Panel on Laboratory Animal Care. Mice were housed in ventilated cages with access to water and normal chow ad libitum. Both male and female mice were used as noted. *Sdhb* exon 3–targeted mice were generated from the International Knockout Mouse Consortium clone Sdhb$^{tm1b(EUCOMM)Hmgu}$ and injected into C57BL6/J blastocytes (12). To delete *Sdhb* in pancreatic β-cells (referred to as SDHB^{βKO}), SDHB$^{fl/fl}$ mice were crossed with the rat insulin promoter-Ins2-Cre mice (MGI 2387567) (Supplementary Fig. 1*A*). To account for the known glucose homeostasis phenotypic effects of the Ins2-Cre transgene, all experiments used Ins2-Cre SDHB$^{fl/wt}$ (referred to as control) (Supplementary Fig. 1*B*–*E*). To sort β-cells, SDHB^{βKO} were crossed with Cre-reporter mice (ROSA$^{mT/mG}$; JAX 007676) (Supplementary Fig. 1*F*).

Islet Isolation
Mouse islets were isolated by pancreatic perifusion of Cizyme (VitaCyte) and digestion at 37°C for 13 min. Islets were purified by Histopaque (Sigma-Aldrich) density gradient centrifugation for 10 min at 850*g* without brake. Islets were collected from the interface, filtered through a 70 μm cell strainer, and cultured overnight in islet medium

(5.6 mmol/L DMEM low glucose containing 4 mmol/L L-glutamine and 1 mmol/L sodium pyruvate, with 10% FBS and 1% penicillin/streptomycin) before selection for experiments.

Assessment of Glucose Homeostasis
All glucose physiology experiments were performed on age- and sex-matched cohorts. To measure glucose tolerance, mice were fasted for 6 h and blood glucose was measured following 2 g/kg intraperitoneal glucose injection. To measure insulin sensitivity, mice were fasted for 4 h and blood glucose was measured following intraperitoneal insulin (0.65 U/kg; Humalog) injection. HOMA of insulin resistance (HOMA-IR) = insulin (pmol/L) × glucose (mmol/L)/22.5; HOMA β-cell function as a percentage (HOMA-β%) = insulin (pmol/L) × 20/glucose (mmol/L) − 3.5.

Insulin Secretion In Vivo and Ex Vivo
To assess GSIS in vivo, mice were fasted for 6 h and blood was collected at indicated times following 2 g/kg intraperitoneal glucose injection. To acquire dynamic insulin secretion profile ex vivo, ∼100 islets/mice were sent to the Vanderbilt Islet Procurement and Analysis Core, and 51 islets/mice at 62.7 islet equivalents equaling 150 μm in diameter were used for islet perifusion. To measure static insulin secretion ex vivo, islets were incubated in 2.8 mmol/L Krebs buffer for 4 h and sequentially stimulated with 5.6 mmol/L and 16.7 mmol/L glucose for 1 h. Islet lysate and medium were collected for insulin measurement (STELLUX Chemi Rodent Insulin ELISA; Alpco).

Measurement of Oxygen Consumption Rate
Respirometry measurements were performed using a Seahorse XFe24 Analyzer (Agilent Technologies) according to the manufacturer's instructions. Briefly, ∼50 islets/mice were seeded in Islet Capture Microplates and incubated in Seahorse XF Media (3 mmol/L glucose and 1% FBS) for 1 h in a CO_2-free 37°C incubator, and oxygen consumption rate (OCR) was measured upon sequential injections of 16.7 mmol/L glucose, 10 μmol/L oligomycin, 10 μm carbonyl cyanide-p-trifluoromethoxyphenylhydrazone (FCCP), and 50 μm rotenone/antimycin A (Agilent Technologies). For a comprehensive measurement of ETC complex activity, islets were permeabilized using Seahorse XF Plasma Membrane Permeabilizer, and OCR was measured as previously described (16). OCR was normalized to protein and presented as relative to control or percent of basal OCR.

ATP/ADP/AMP Measurement
Intracellular adenine nucleotides were extracted from ∼50 islets/mice and measured using the ATP/ADP/AMP Assay Kit (catalog number A-125; Biomedical Research Service) and a SpectraMax iD5 Microplate Reader.

Flow Cytometry

To measure mitochondrial activity in mouse β-cells, isolated islets from Ins-Cre2 ROSA$^{mT/mG}$, SDHB$^{f/f}$, or SDHB$^{f/wt}$ mice were incubated in 5.6 mmol/L and 16.7 mmol/L glucose for 4 h, dissociated, resuspended in FACS buffer (5% FBS/PBS), and loaded with 50 nmol/L tetramethylrhodamine, ethyl ester, perchlorate (TMRE; Thermo Fisher Scientific) for 1 h at 37°C. GFP-positive cells were gated, and TMRE signal was analyzed on a BD LSR II flow cytometer. Data were analyzed using FlowJo.

Untargeted Liquid Chromatography-Mass Spectrometry Metabolic Profiling

Metabolic profiling was performed at Northwest Metabolomics Research Center. Briefly, isolated islets were homogenized in MeOH/H$_2$O (80:20). Supernatant was dried in a vacufuge and reconstituted in HILIC solvent (30% mobile phase A/70% mobile phase B) before analysis on an LC-QQQ system coupled to a SCIEX 6500+ triple quadrupole mass spectrometer operating in multiple reaction monitoring mode through the Analyst 1.6.3 software. Metabolite concentrations were quantified in a relative manner using Multiquant 3.0 software and normalized to total peak sum.

RNA Sequencing and Bioinformatic Analysis

Total RNA was extracted from ∼200 islets/mice by TRIzol extraction followed by RNeasy Plus Micro Kit (Qiagen). A cDNA library was prepared with the TruSeq Stranded Total RNA Kit and sequenced using an Illumina HiSeq 4000. Gene-level quantification was performed on all samples' sorted BAM files using FeatureCounts, counted by Gencode-defined exons, and aggregated to the gene level. Differential expression analyses were performed with edgeR to generate reads per kilobase of transcript per million mapped reads values. Gene set enrichment analysis (GSEA) was performed on MSigDB annotated gene sets with more than one read per kilobase of transcript per million mapped reads in all replicates. Pathway enrichment analyses of genes differentially expressed ($P < 0.05$) were performed with the integrated knowledge database software MetaCore (Clarivate Analytics).

Immunoblotting

Isolated islets were lysed in protease and phosphatase inhibitor–supplemented radioimmunoprecipitation assay buffer and immunoblotted as previously described (17). The following primary antibodies were used: phosphorylated ribosomal protein S6 (p-S6; Catalog no. 4858), phosphorylated AMPKa (Catalog no. 2537), SDHA (Catalog no. 11998) (Cell Signaling Technology); OxPhos Cocktail (ab110413); and b-actin (A5316; Sigma-Aldrich). Antibodies were detected with IRDyes and scanned on the Odyssey CLx (LI-COR Biosciences). Relative band intensity was quantified using Odyssey Image Studio 2.0.

Histological Analysis

Immunofluorescence staining was performed as previously described (17). Processed tissue sections were incubated in primary antibody at 4°C overnight: SDHB (ab14714; sc-271548), sirtuin 5 (Sirt5; Catalog number 8779), lysine succinylation (K-Succ; PTM-401), and p-S6. For each antigen, immunostaining of pancreas sections from experimental groups was performed in parallel and imaged with fixed settings on the Leica DM IL LED microscope to reflect differences in protein. For morphometric analysis, area measurements and signal intensities were quantified in 5–10 islet images/mouse from $n = 3$ mice/genotype using Volocity 6.3 by an observer blinded to experimental groups.

β-Cell Replication

β-Cell replication was assessed in pancreas sections and isolated islets as previously described (18). Replication was analyzed using a Cellomics ArrayScan VTi.

Transmission Electron Microscopy

Excised pancreata were harvested, fixed in 2.5% glutaraldehyde in 0.1 mol/L cacodylate buffer (pH 7.4), processed, and imaged using a JEOL JEM1400 Digital Capture transmission electron microscope at the Stanford University Cell Sciences Imaging Facility.

Rapamycin Administration

Rapamycin (LC Laboratories) was dissolved in DMSO (100 mg/mL stock). For in vitro experiments, isolated islets were incubated with 50 nmol/L rapamycin or vehicle for 24 h. For in vivo studies, rapamycin stock was diluted to 1 mg/mL in 10% polyethylene glycol 400/10% Tween-80 (vehicle). Following intraperitoneal injection of 5 mg/kg rapamycin or vehicle, glucose tolerance test (GTT) and in vivo GSIS assays were performed 1 h postinjection.

Statistical Analysis

Results are presented as the mean ± SD or SEM. Statistical comparisons were performed using Student t test or two-way ANOVA where appropriate (GraphPad), and significance was defined by $P < 0.05$. Details of sample size and independent experimental repeats are provided in the figure legends.

Data and Resource Availability

All data from this study are presented in the published article and the supplementary materials. Additional information is available from the corresponding author upon request.

RESULTS

SDH Is Reduced in Islets From Patients With Diabetes

Loss of SDH activity and expression occurs in the peripheral tissues of diabetic rodents and patients with T2D (19–21). Moreover, SDHB is downregulated in prediabetic islets from high-fat diet mice and obese *ob/ob* mice (22). However, it is unknown whether SDH expression and/or activity is altered in T2D β-cells. To address this question,

we evaluated SDHB expression in human pancreatic sections from healthy ND and T2D donors (Supplementary Table 1). While SDHB was expressed in both insulin-positive β-cells and insulin-negative acinar tissue of ND donors (Supplementary Fig. 2), SDHB expression was significantly lower in β-cells of T2D donors (Fig. 1A and B). By contrast, expression of NDUFB8, a complex I–associated mitochondrial protein, was not significantly changed in T2D β-cells (Fig. 1C), consistent with a relatively selective reduction of SDH. Recently, nonenzymatic K-Succ was identified as a consequence of excess succinate accumulation in the context of SDH loss (23), and the accumulation of K-Succ is counterregulated by the desuccinylase enzyme SIRT5 (24). Although K-Succ was not increased in T2D donor islets (Fig. 1D), a robust increase in SIRT5 expression was observed (Fig. 1E), potentially indicating a compensatory upregulation of desuccinylation activity. The findings of reduced SDHB and increased SIRT5 protein in human T2D β-cells raised the possibility that reduced SDH enzyme activity causally contributes to T2D development.

β-Cell–Specific Deletion of SDHB Leads to Pubertal Diabetes

To investigate the function of SDH in β-cells, we conditionally disrupted SDHB in the β-cells of mice (SDHB^βKO) (Fig. 2A). β-Cell–selective loss of SDHB expression within the islet was confirmed by immunostaining of pancreatic tissue (Fig. 2B and Supplementary Fig. 1G) and Western blotting of isolated islets (Fig. 2C). Because the SDH complex participates in both the ETC and TCA cycle, the functional impact of SDHB disruption on these metabolic pathways was evaluated. First, we evaluated mitochondrial ETC complex (CI–CIV) activity using a Seahorse bioanalyzer. Notably, SDHB^βKO islets demonstrated nearly undetectable CII activity, but no significant change in other ETC complex activities (Fig. 2D). Hence, disruption of CII was not functionally associated with collateral disruption of or compensation by other ETC complexes. Next, we evaluated SDH activity by measuring intracellular succinate levels by mass spectrometry. Indeed, SDHB^βKO islets had significantly elevated succinate levels (Fig. 2E). Consistent with the robust increase in intracellular succinate, SDHB^βKO β-cells exhibited significantly increased protein K-Succ (Fig. 2F) and a robust increase in expression of the desuccinylation enzyme SIRT5 (Fig. 2G). Together, these data confirm β-cell–specific deletion of SDH catalytic activity in our mouse model and uncover excess succinate accumulation and protein hypersuccinylation as functional consequences of SDH deficiency in β-cells (25).

To study the in vivo effects of β-cell SDHB deficiency on glucose homeostasis, we measured blood glucose levels in control and SDHB^βKO littermates from weaning (3 weeks) to 20 weeks of age. Loss of β-cell SDHB expression led to a progressive rise in fed glucose levels, with no sex-specific or body weight effects (Fig. 3A and Supplementary Fig. 1H and I). While young SDHB^βKO mice were

normoglycemic and normoinsulinemic until 6 weeks, hyperglycemia was evident by 10 weeks, and overt insulinopenic diabetes (403.8 ± 92.87 mg/dL) was established by 20 weeks (Fig. 3B and C). SDHB^βKO mice at 20 weeks also demonstrated increased fasting glucose levels and inappropriately low fasting serum insulin levels, confirming a diabetic phenotype (Fig. 3D and E). Consistent with a β-cell–selective defect, HOMA-IR was unchanged, while HOMA-β% was significantly reduced in diabetic SDHB^βKO mice (Fig. 3F and G). Similar to human and other mouse models of diabetes (26,27), SDHB^βKO mice demonstrated a progressive reduction in β-cell mass without alterations in α-cell mass (Fig. 3H), which further supported a pure β-cell defect. Next, we examined the impact on β-cell ultrastructure by transmission electron microscopy. At 5 weeks, SDHB^βKO and control littermates demonstrated no apparent differences in mature insulin granules with an electron-dense core or mitochondrial morphology (Fig. 3I and J). However, by 20 weeks, SDHB^βKO islets exhibited large membraned vacuoles containing engulfed organelles, including insulin granules and damaged mitochondria (Fig. 3J), a T2D-associated finding related to autophagy dysregulation (28). Collectively, these data indicate that β-cell–specific disruption of SDHB resulted in insulinopenic diabetes in pubertal-age mice.

SDHB^βKO Mice Exhibit Impaired GSIS, β-Cell Replication, and Mitochondrial Function

To identify the mechanism that drives SDHB-deficient β-cell dysfunction and diabetes, we focused our analysis on prediabetic 5-week-old mice. First, we interrogated the ability of SDHB^βKO mice to handle glucose challenges by intraperitoneal GTT. Compared with control littermates, young SDHB^βKO mice were mildly glucose intolerant (Fig. 4A) with unchanged insulin sensitivity (Fig. 4B). SDHB^βKO mice exhibited reduced insulin release following glucose administration (Fig. 4C and D). Next, we directly evaluated the impact of SDHB disruption on insulin secretion by performing dynamic islet perifusion assays. SDHB^βKO islets failed to secrete insulin in response to leucine (consistent with impaired TCA cycle metabolism) and demonstrated reduced glucose-stimulated first- and second-phase insulin secretion (Fig. 4E). Importantly, exendin-4–augmented insulin secretion was slightly impaired, while potassium chloride–induced insulin secretion by SDHB^βKO was not significantly altered, indicating an intact insulin secretion mechanism downstream of mitochondrial metabolism (Fig. 4E and Supplementary Fig. 3A). Furthermore, control and SDHB^βKO islets demonstrated similar insulin content (Supplementary Fig. 3B), indicating an intact insulin expression and storage in prediabetic islets.

Given the role of mitochondrial metabolism in regulating β-cell replication (4) and our observation of reduced β-cell mass in prediabetic SDHB^βKO mice, we predicted that impaired glucose-stimulated β-cell expansion contributed to the diabetic phenotype of SDHB^βKO mice. In fact, while
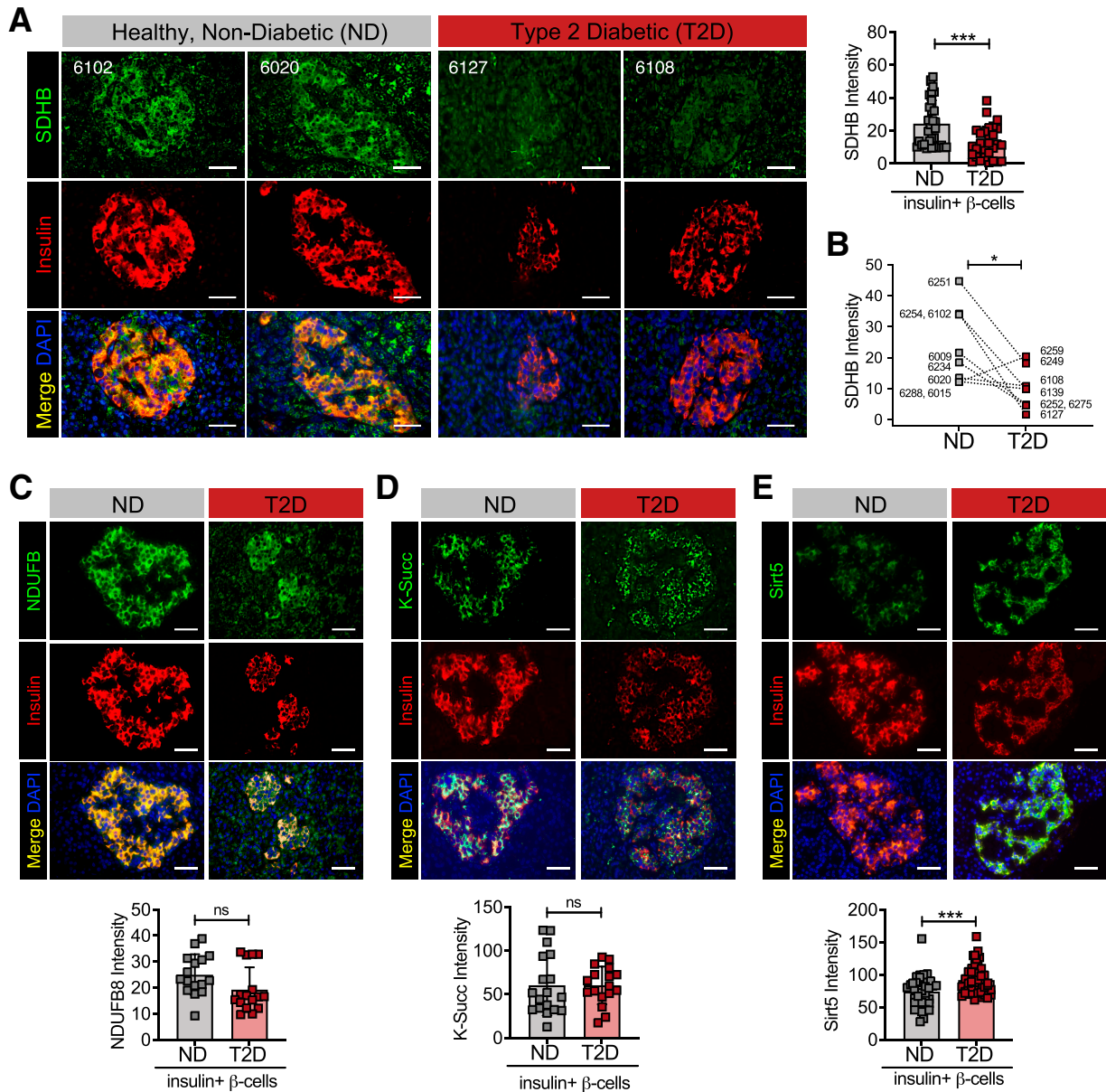
Figure 1—SDHB expression is reduced in human diabetic β-cells. *A*: Representative immunofluorescent images of pancreatic sections from healthy ND and T2D human donors immunostained for insulin (red) and SDHB (green). Quantification of mean SDHB staining intensity within the insulin$^+$ β-cells of individual donors is shown in adjacent graph (n = 4–6 islets/donor from n = 7–8 donors/group). *B*: Age-, sex-, and BMI-matched comparison of the mean SDHB staining intensity within the insulin$^+$ area (n = 7–8 donors/group). Donor identification information is provided (Supplementary Table 1). Representative immunofluorescent images of pancreatic sections from ND and T2D stained for insulin (red) and NDUFB8 (*C*, green), K-Succ (*D*, green), and SIRT5 (*E*, green). Quantification of mean staining intensity ± SD within insulin$^+$ β-cells are shown in adjacent graphs (n = 4–8 donors/group). Data represented as mean immunofluorescence ± SD and analyzed by unpaired (*A*) or paired *t* tests (*B–E*). *$P < 0.05$; ***$P < 0.001$. Scale bars, 100 μm.

basal β-cell replication was unchanged, glucose-stimulated β-cell replication was significantly impaired in prediabetic SDHB$^{\beta KO}$ islets compared with controls (Fig. 4*F*). These results indicate a failure of compensatory nutrient-stimulated β-cell expansion with the loss of SDHB (26).

Knowing that GSIS and replication were disrupted, we next investigated the impact of SDH dysfunction on mitochondrial regulation of stimulus-secretion coupling. To

assess mitochondrial glucose metabolism, we measured OCR in response to glucose stimulation. In control islets, injection of 16.7 mmol/L glucose significantly increased OCR by 4-fold (Fig. 4*G*), and mitochondrial uncoupling with FCCP increased OCR by 2.2-fold above the basal rate, resulting in a spare reserve capacity of ~225% (Fig. 4*H*). By contrast, SDHB$^{\beta KO}$ islets exhibited reduced basal and glucose-stimulated respiration (Fig. 4*G*) and reduced
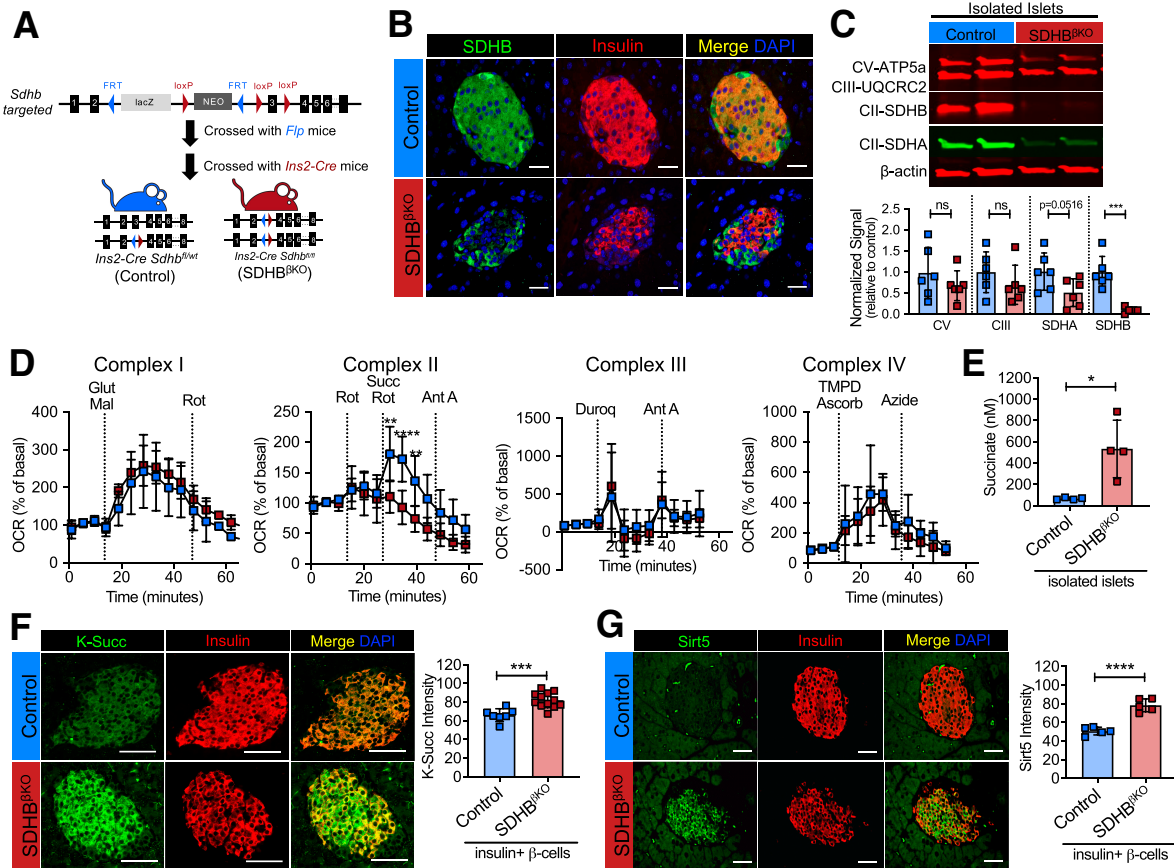
Figure 2—Loss of SDHB impairs mitochondrial CII activity, increases succinate, and results in β-cell hypersuccinylation. *A*: Schematic of the targeting strategy used to generate a β-cell–specific SDHB knockout mice (SDHB$^{\beta KO}$). The *sdhb* gene targeting vector contained a neomycin cassette (NEO) flanked by Frt sites followed by exon 3 flanked by LoxP sites. *Sdhb*-targeted mice were bred with Flp deleter mice and then Ins2-Cre mice to generate SDHBβKO mice. Control mice were either Ins2-Cre SDHB$^{fl/wt}$ (all in vivo studies) or occasionally Cre-neg SDHB$^{fl/wt}$ (some in vitro studies). *B*: Representative immunofluorescent images of SDHB in pancreatic sections from control and SDHB$^{\beta KO}$ mice. *C*: Representative immunoblot of OxPhos proteins in islet lysates from control and SDHB$^{\beta KO}$ ($n = 6$ mice/group). Quantification of OxPhos protein (CIII and CV) and SDH subunit (SDHA and SDHB) expression normalized to β-actin loading control. *D*: Measurement of mitochondrial respiratory activity of CI–IV in islets from control ($n = 5$) and SDHB$^{\beta KO}$ ($n = 6$) mice from two independent experiments. *E*: Succinate level in control and SDHB$^{\beta KO}$ islets measured by LC-MS ($n = 4$ mice/group). Representative immunofluorescent images of K-Succ (*F*, green) and SIRT5 (*G*, green) staining in pancreatic sections from control and SDHB$^{\beta KO}$ mice. Quantification of mean staining intensity ± SD within insulin$^+$ β-cells are shown in adjacent graphs in *F* and *G* ($n = 5$ mice/group). Data represented as mean ± SD analyzed by two-way ANOVA with Sidak posttest (*D*) or unpaired *t* test (*E–G*). *$P < 0.05$; ***$P < 0.001$; ****$P < 0.0001$. Scale bars, 100 μm. Ant A, antimycin A; Ascorb, ascorbate; Duroq, duroquinone; Glut, glutamine; Mal, malate; Rot, rotenone; Succ, succinate; TMPD, N,N,N′,N′-tetramethyl-para-phenylene-diamine.

maximal respiration and spare reserve capacity (Fig. 4*H*). The lack of spare reserve capacity confirms disruption of SDH activity (29), while altered OCR measurements of SDH-independent parameters implicate a collateral impact on ATP generation and glucose metabolism, despite intact ETC CI, CIII, and CIV (interrogated above). Indeed, SDHB$^{\beta KO}$ islets demonstrate a >50% reduction in ATP synthase–related OCR following oligomycin injection (Fig. 4*G*). To directly assess ATP generation capacity, we measured ATP and ADP levels following glucose stimulation. Whereas exposure of control islets to glucose elevation increased the ATP to ADP ratio by twofold, glucose-exposed SDHB$^{\beta KO}$ islets failed to increase the ATP to ADP

ratio (Fig. 4*I*). These data indicate that SDHB$^{\beta KO}$ β-cells have respiratory deficits that contribute to reduced ATP generation and, consequently, reduced GSIS.

To evaluate the β-cell–specific mitochondrial consequences of SDH complex disruption, we crossed Ins2-Cre SDHB$^{\beta KO}$ mice to Cre-reporter mice (ROSA$^{mT/mG}$) and specifically analyzed GFP-positive β-cells (Fig. 4*J*). Isolated islets from ROSA$^{mT/mG}$ control and SDHB$^{\beta KO}$ mice were loaded with a mitochondrial membrane potential (ΔΨm)–dependent probe, TMRE, to assess mitochondrial activity in GFP-gated β-cells by flow cytometry. As anticipated, control β-cells demonstrated increased ΔΨm in response to high glucose exposure

/processing-instruction())">

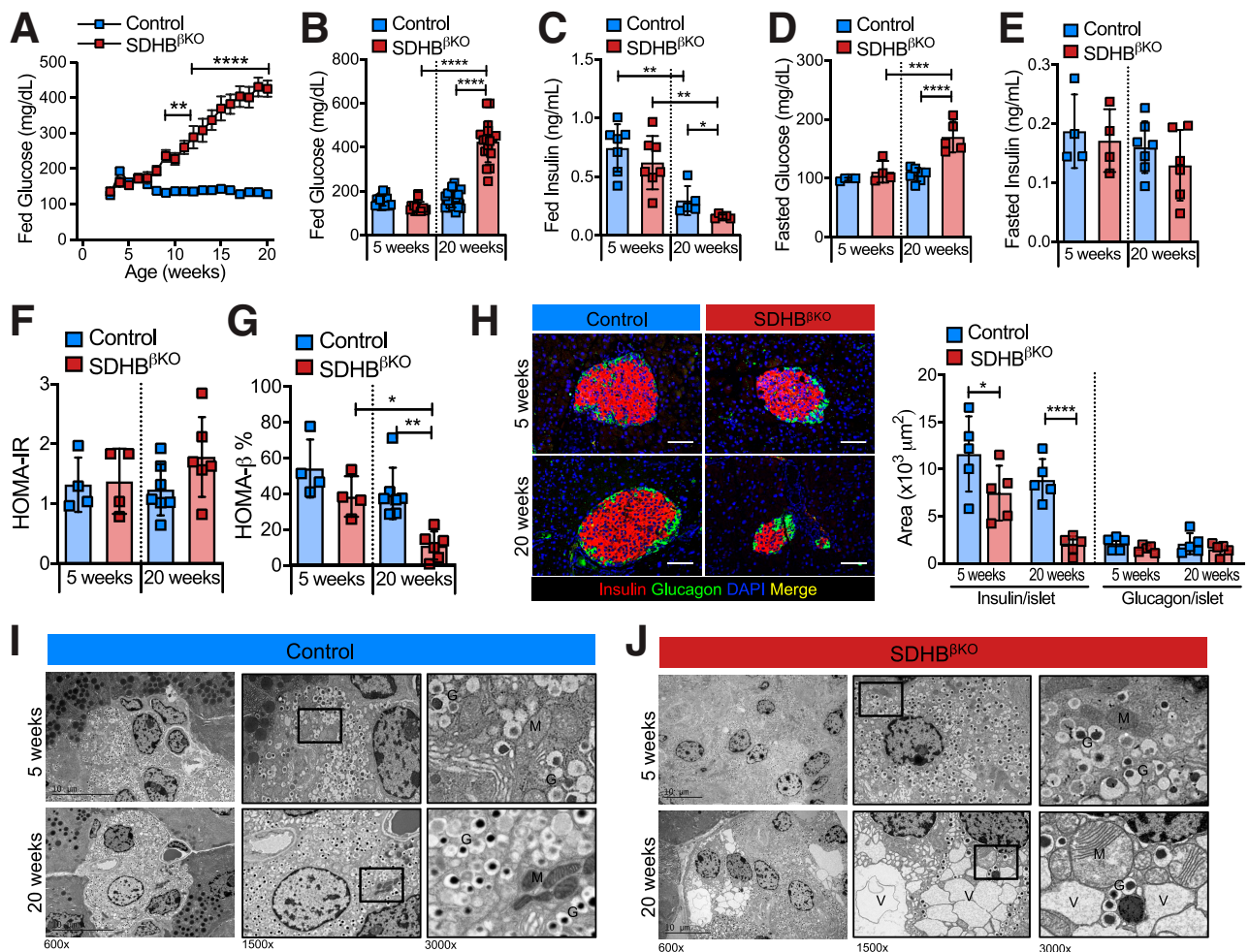**Figure 3**—SDHB$^{\beta KO}$ mice develop early-onset insulinopenic diabetes. *A*: Free-fed blood glucose levels in Ins2-Cre SDHB$^{fl/wt}$ (control; *n* = 15) and SDHB$^{\beta KO}$ (*n* = 17) mice (3–20 weeks). Data represented as mean ± SEM. Free-fed blood glucose (*B*, mg/dL) and serum insulin (*C*, ng/mL) in 5- and 20-week-old control and SDHB$^{\beta KO}$ mice (*n* = 15–21/group). Sixteen-hour–fasted blood glucose (*D*) and serum insulin (*E*) levels in control and SDHB$^{\beta KO}$ mice (*n* = 4–7/group). Calculated HOMA-IR (*F*) and HOMA-β% (*G*) in 5- and 20-week-old control and SDHB$^{\beta KO}$ mice (*n* = 4–7/group). *H*: Representative immunofluorescent images pancreatic sections from control and SDHB$^{\beta KO}$ mice stained with insulin (red) and glucagon (green). Nuclei were counterstained with DAPI. Scale bars, 50 μmol/L. Quantification of insulin and glucagon positive areas per islet in pancreatic sections from control and SDHB$^{\beta KO}$ mice are shown in the adjacent graph in *H* (*n* = 5/group). Representative transmission electron micrographs of control (*I*) and SDHB$^{\beta KO}$ (*J*) islet β-cells from 5- and 20-week-old mice. Areas shown in the magnified images are boxed. G, insulin granules; M, mitochondria; V, vacuolar compartments. Data represented as mean ± SD (unless specified) and were analyzed by two-way ANOVA with Sidak posttest (*A*) or one-way ANOVA with Tukey posttest (*B–G*). *$P <$ 0.05; **$P <$ 0.01; ***$P <$ 0.001; ****$P <$ 0.0001.

(Fig. 4*K*). By contrast, SDHB$^{\beta KO}$ β-cells had elevated $\Delta\Psi$m (hyperpolarization) under basal conditions that collapsed upon elevated glucose exposure (Fig. 4*K*). This paradoxical loss of $\Delta\Psi$m indicates an inability to maintain the mitochondrial electron gradient under high glucose, which is consistent with the reduced glucose-stimulated ATP generation of SDHB$^{\beta KO}$ β-cells and, potentially, accumulation of succinate within the mitochondria (30). Together, these results demonstrate that β-cell disruption of SDH robustly impairs mitochondrial bioenergetics, stimulus-coupled insulin secretion, and compensatory β-cell replication, thereby culminating in diabetes development.

Loss of SDHB Perturbs β-Cell Metabolism and Induces Mammalian Target of Rapamycin Hyperactivation

The abnormal $\Delta\Psi$m of SDHB$^{\beta KO}$ β-cells is indicative of altered cellular metabolism (31). Specifically, aberrant mitochondrial hyperpolarization has been associated with metabolic substrate overload (32), leading us to hypothesize that the basal hyperpolarization of SDHB$^{\beta KO}$ β-cells reflected significant metabolic perturbation. To investigate this, we performed comparative metabolomics (liquid chromatography-mass spectrometry [LC-MS]) and high-throughput transcriptome (RNA-sequencing) analysis in islets (Fig. 5*A*). Notably, SDHB$^{\beta KO}$ islets demonstrated prominent accumulation of succinate (as anticipated) with
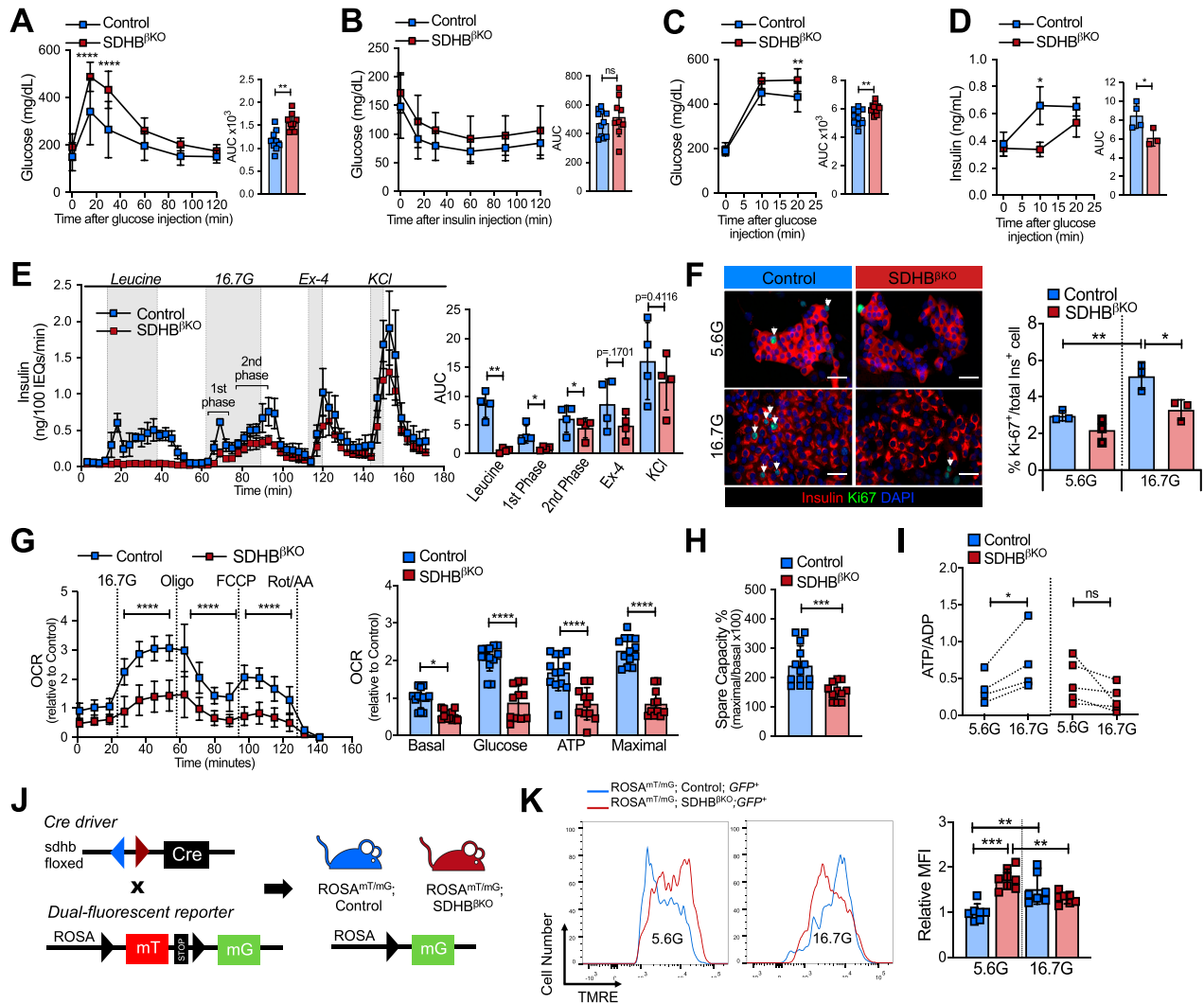
Figure 4—Prediabetic SDHB-deficient β-cells fail to induce insulin secretion, replication, and mitochondrial activity in response to glucose. Glucose levels following 2 mg/kg intraperitoneal glucose (*A*) and 0.75 IU/kg intraperitoneal insulin (*B*) administration in 5-week-old Ins2-Cre SDHB$^{fl/wt}$ (control) and SDHB^{βKO} mice (*n* = 9/group). Corresponding area under the curve (AUC) plots are shown at right. In vivo GSIS (glucose 10 mg/kg) showing glucose (*C*) and serum insulin (*D*) levels in 5-week-old control and SDHB^{βKO} mice (*n* = 10/group). Corresponding AUC plots are shown at right. *E*: Insulin secretion in response to 10 mmol/L leucine, 16.7 mmol/L glucose, 20 nmol/L exendin-4 (Ex-4), and 20 mmol/L KCl in isolated islets from 5-week-old control and SDHB^{βKO} mice (*n* = 4/group) from two independent experiments. AUCs of individual treatment conditions are shown at right. *F*: Representative immunofluorescent images of dispersed islet cells from 5-week-old control and SDHB^{βKO} mice stained with insulin (red) and Ki-67 (green) after 72-h incubation with 5.6 mmol/L glucose (5.6G) and 16.7 mmol/L glucose (16.7G). Arrowheads indicate Ki-67$^+$ β-cells. Quantification of Ki-67$^+$ cells in insulin$^+$ cells are shown in adjacent graph (*n* = 9 independent wells from 3 mice/group). *G*: Measurement of OCR upon sequential injections of 16.7G, oligomycin (Oligo), FCCP, and rotenone/antimycin A (Rot/AA) in isolated islets from 5-week-old control (*n* = 13) and SDHB^{βKO} (*n* = 11) mice from three independent experiments. Calculated OCR values for respiratory parameters are shown in the adjacent graph. *H*: Calculated spare reserve capacity (maximum/basal × 100%) in 5-week-old control and SDHB^{βKO} islets. *I*: ATP/ADP ratio of control and SDHB^{βKO} islets exposed to 5.6G and 16.7G (*n* = 4 mice/group from four independent experiments). *J*: Schematic of the targeting strategy to generate β-cell fluorescent Cre-reporter mice. *K*: Representative FACS analyses of mitochondrial membrane potential (TMRE) in of GFP$^+$ β-cells from dispersed 5-week-old ROSA^{mTmG} control and ROSA^{mTmG} SDHB^{βKO} islets after a 2-h exposure to 5.6G and 16.7G. Median fluorescence intensity (MFI) of TMRE relative to 5.6G control is shown in the adjacent graph in *K* (*n* = 7–8 mice/group from three independent experiments). Data represented as mean ± SD and were analyzed by two-way ANOVA with Sidak posttest (*A–D*), one-way ANOVA with Tukey posttest (*F*, *G*, and *K*), unpaired *t* test (AUC plots, *H*), or paired *t* test (*I*). *$P < 0.05$; **$P < 0.01$; ***$P < 0.001$; ****$P < 0.0001$. IEQ, islet equivalents equaling 150 μm in diameter.

no change in fumarate levels, fatty acid intermediates, nucleic acid building blocks, and precursors of protein synthesis despite a deficit of free amino acid pools (Supplementary Fig. 4*A* and *B*). Calculated differential abundance scores demonstrated an upregulation of several anabolic pathway intermediates, including fatty acid/lipid, sugar, and nucleotide metabolites (Supplementary Fig. 4*C*). Similarly, MetaCore analysis indicated that lipid
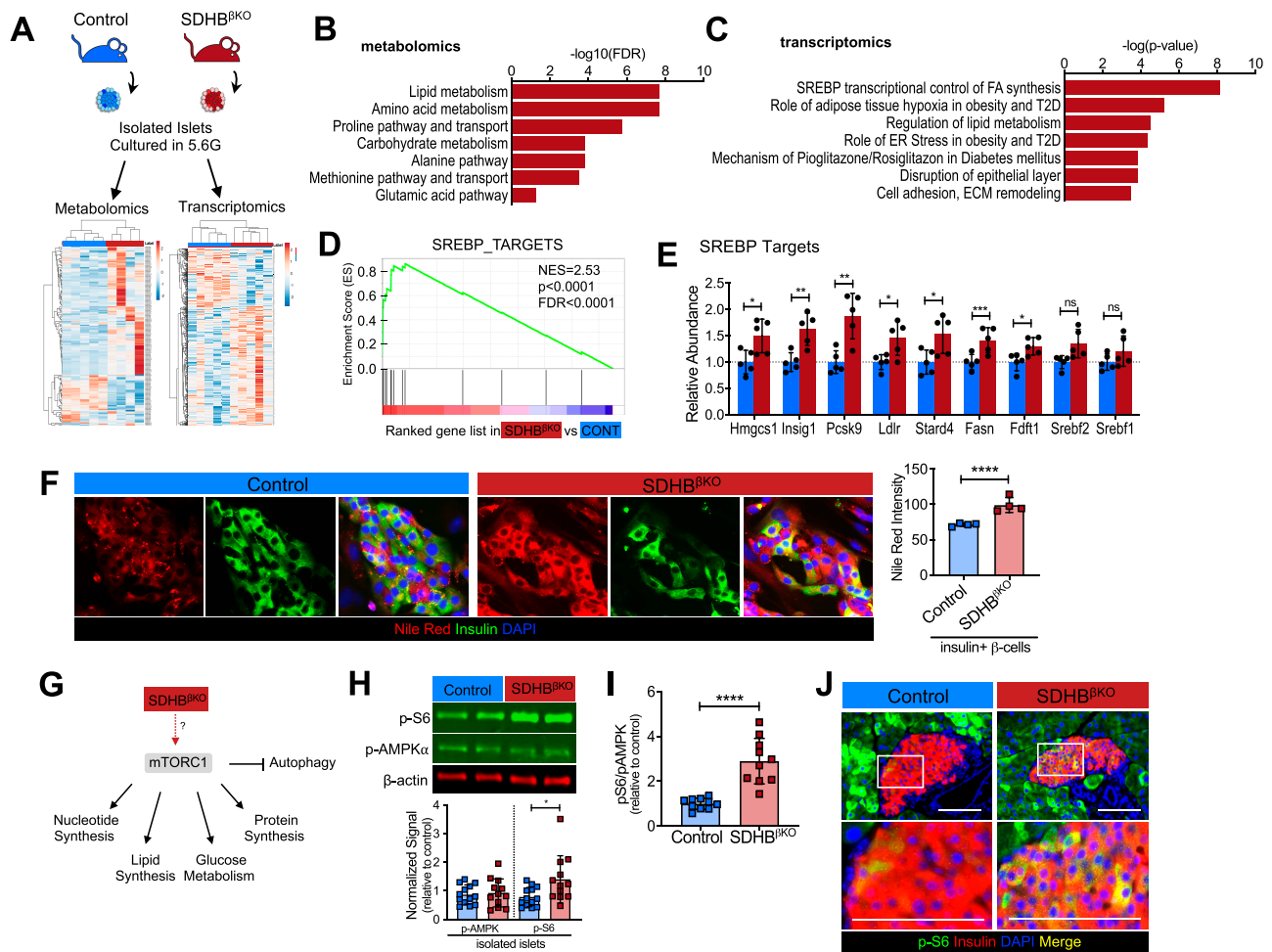
Figure 5—SDHB^βKO islets have mTOR hyperactivation and increased SREBP-regulated lipid metabolism. A: Graphical representation of metabolomics and transcriptomics experiments. Heat map using Euclidean distance as the metric of resting isolated islets from 5-week-old Ins2-Cre SDHB^fl/wt (control) and SDHB^βKO mice (n = 5/group). Significantly altered metabolic (B) and transcriptional (C) pathways in SDHB^βKO islets determined by MetaCore analysis. D: GSEA analyses of SREBP target genes comparing SDHB^βKO to control. E: Transcript expression levels of SREBP target genes. F: Representative immunofluorescent images of dispersed islet cells from control and SDHB^βKO mice stained with Nile Red (red) and insulin (green) after 72 h incubation with 5.6 mmol/L glucose (5.6G). Nuclei were counterstained with DAPI. Quantitation of mean Nile Red intensity in insulin^+ cells is shown in adjacent graph in F (n = 4–5 images from 4 mice/group). G: Graphical representation of our working hypothesis that SDH disruption activates mTORC1-regulated anabolic pathways. H: Representative immunoblot and quantification of p-S6 and phosphorylated (p-)AMPKα protein expression of islet lysates from 5-week-old Ins2-Cre SDHB^fl/wt or Cre-neg (control) and SDHB^βKO mice (n = 9–10/group). Quantification of p-S6 and p-AMPKα expression normalized to β-actin loading control shown at bottom. I: Ratio of p-S6 over p-AMPKα. J: Representative immunofluorescent images of p-S6 staining in pancreatic sections from 5-week-old control and SDHB^βKO mice. Boxes indicate areas of higher magnification images shown below. Note p-S6 expression in insulin^+ areas of SDHB^βKO mice. Scale bars, 100 μm. Data represented as mean ± SD and were analyzed by unpaired t test (E, F, H, and I). *$P < 0.05$; **$P < 0.01$; ***$P < 0.001$; ****$P < 0.0001$. ECM, extracellular matrix; ER, endoplasmic reticulum; FA, fatty acid; FDR, false discovery rate; NES, normalized enrichment score.

metabolism and amino acid metabolism were the most significantly altered pathways in SDHB^βKO islets (Fig. 5B). These data suggest that loss of SDH triggered an unexpected shift toward cellular anabolism in the setting of reduced cellular energetics.

Accordingly, transcriptomic analysis identified gene signatures of metabolic perturbation in SDHB^βKO islets. Comparable levels of "housekeeping" and islet cell-type identity (α, β, δ, and ɣ cells) islet genes demonstrated intact

cellular identity (Supplementary Fig. 5). Consistent with metabolomics data, MetaCore transcriptional analysis identified fatty acid, lipid, and cholesterol metabolism pathways, including SREBP-regulated cholesterol and fatty acid biosynthesis, as the most significantly altered pathways in SDHB^βKO islets (Fig. 5C). In line with this finding, GSEA revealed that SREBP target genes were enriched in SDHB^βKO islets (Fig. 5D), with *Hmgcs1*, *Insig1*, *Psk9*, *Stard4*, and *Fasn* among the induced genes (Fig. 5E). Upregulation

of these lipogenic genes highlights a potential effect of SDH disruption on SREBP-regulated lipid synthesis. Indeed, examination of lipid content with a lipophilic dye, Nile Red, revealed strong and diffuse staining in insulin-expressing β-cells from SDHB$^{\beta KO}$ that was distinct from the punctate lipid droplet staining in control β-cells (Fig. 5F). These observations demonstrate an inappropriate increase in lipid accumulation in SDHB$^{\beta KO}$ islets under basal conditions (33) without major effects on alternative metabolic pathways, such as glycerol-3-phosphate and malate-aspartate shuttles (Supplementary Fig. 6). Together, these data further support our hypothesis that loss of SDH triggers a shift toward lipid anabolism.

Prior work has shown the mammalian target of rapamycin complex 1 (mTORC1) pathway is hyperactivated in SDH-deficient tumors (34) and that mTOR activates SREBP, a key regulator of rate-limiting lipogenic gene expression, by inducing SREBP cleavage and nuclear localization (35). Therefore, we hypothesized that mTORC1, a master regulator of cell growth and metabolism that promotes anabolic processes (36), was hyperactivated in SDHB-deficient β-cells (Fig. 5G). Consistent with this view, p-S6, a target of mTORC1 signaling, was significantly increased in SDHB$^{\beta KO}$ islets (Fig. 5H). By contrast, AMPK functions as an opposing nutrient sensor that promotes catabolism in response to nutrient deficiency (36). Despite the low energetic state of SDHB$^{\beta KO}$ islets, where AMPK pathway activation was anticipated, SDHB$^{\beta KO}$ islets demonstrated persistent hyperactivation of the mTORC1 relative to AMPK pathway (Fig. 5I). Additionally, mTORC1 hyperactivation (p-S6) was confined to the β-cell population of the islet (Fig. 5J). Taken together, these data indicate mTORC1 pathway hyperactivation in SDHB$^{\beta KO}$ β-cells.

The observed mTORC1 hyperactivation and anabolic metabolite excess in SDHB$^{\beta KO}$ islets led us to test whether the functional defects of SDHB$^{\beta KO}$ islets would be reversed by the mTORC1 inhibitor rapamycin, known to reprogram mitochondrial metabolism (37). First, we assessed the effects of rapamycin on the glucose-stimulated $\Delta \Psi$m of GFP$^+$ control and SDHB$^{\beta KO}$ β-cells (Fig. 6A and B). In basal glucose conditions, acute treatment of rapamycin had limited effects on control β-cells but significantly mitigated the hyperpolarization phenotype of SDHB$^{\beta KO}$ β-cells (Fig. 6A and B). Additionally, the paradoxical loss of $\Delta \Psi$m with high glucose exposure was rescued by rapamycin treatment in SDHB$^{\beta KO}$ β-cells. This led us to hypothesize that under basal conditions, SDH disruption elevates succinate, which drives mTOR hyperactivation, and that rapamycin rescues this phenotype by reducing succinate levels. Indeed, our studies in vitro demonstrate that rapamycin reduces succinate levels and lowers $\Delta \Psi$m in R7T1 β-cells treated with either the irreversible SDH inhibitor 3-nitroprorionic acid or cell-permeable succinate dimethyl succinate (Supplementary Fig. 7). Therefore, excess mTOR pathway activation

substantially contributed to the abnormal SDHB$^{\beta KO}$ β-cell mitochondrial phenotype.

The rapamycin rescue of SDHB$^{\beta KO}$ β-cell mitochondrial activity raised the possibility that mTOR inhibition might also improve the defective stimulus-secretion coupling of these β-cells. To test this hypothesis, we performed static islet GSIS assay after treatment with rapamycin. Both vehicle- and rapamycin-treated control islets demonstrated an approximate fourfold increase in glucose-induced insulin secretion (Fig. 6C). Vehicle-treated SDHB$^{\beta KO}$ islets demonstrate impaired GSIS; however, rapamycin treatment significantly enhanced insulin secretion under high glucose with no significant changes at resting glucose levels (Fig. 6C), resulting in an approximate threefold improvement of the stimulation index (Fig. 6D). These data confirmed a rescue of the SDHB$^{\beta KO}$ β-cell metabolic phenotype by mTOR inhibition.

Next, we tested the in vivo effects of rapamycin on β-cell function by performing GTTs and GSIS tests on control and SDHB$^{\beta KO}$ mice. To avoid the detrimental impacts of chronic rapamycin treatment on β-cell function and peripheral insulin resistance (38), we examined the acute effect of rapamycin (1 h) on glucose homeostasis. We conducted a crossover experiment in which control and SDHB$^{\beta KO}$ were subjected to GTT and GSIS assays 1 h after intraperitoneal vehicle or rapamycin (5 mg/kg) injection (Fig. 6E). A crossover design was used to control for the phenotypic variability of individual mice. Consistent with in vitro data, acute rapamycin treatment had no effect on glucose tolerance (Fig. 6F) or insulin secretion in control animals (Supplementary Fig. 8A). By contrast, a single dose of rapamycin treatment marginally improved the glucose intolerance of SDHB$^{\beta KO}$ mice, and this modest glucose homeostasis improvement was accompanied by increased insulin secretion following glucose administration (Fig. 6F and Supplementary Fig. 8B). Specifically, the insulin secretion index of rapamycin-treated SDHB$^{\beta KO}$ mice was comparable to that of vehicle- or rapamycin-treated control mice (Fig. 6G). Together, these data demonstrate that rapamycin acutely improves mitochondrial function, glucose tolerance, and GSIS in the context of SDH deficiency–related mTORC1 hyperactivation.

DISCUSSION

SDH/CII complex is at the nexus of mitochondrial bioenergetics and cellular metabolism, but its function in β-cells has not been extensively studied. In the current study, we demonstrate a central role for SDH in regulating β-cell mitochondrial metabolism and identify SDH deficiency as a potential contributing factor to progressive β-cell failure in T2D.

Protein expression of SDHB, a surrogate marker for the SDH complex, is downregulated in the β-cells of human patients with T2D. This observation is consistent with reduced transcriptomic expression of oxidative phosphorylation-related genes in tissue biopsies from patients with
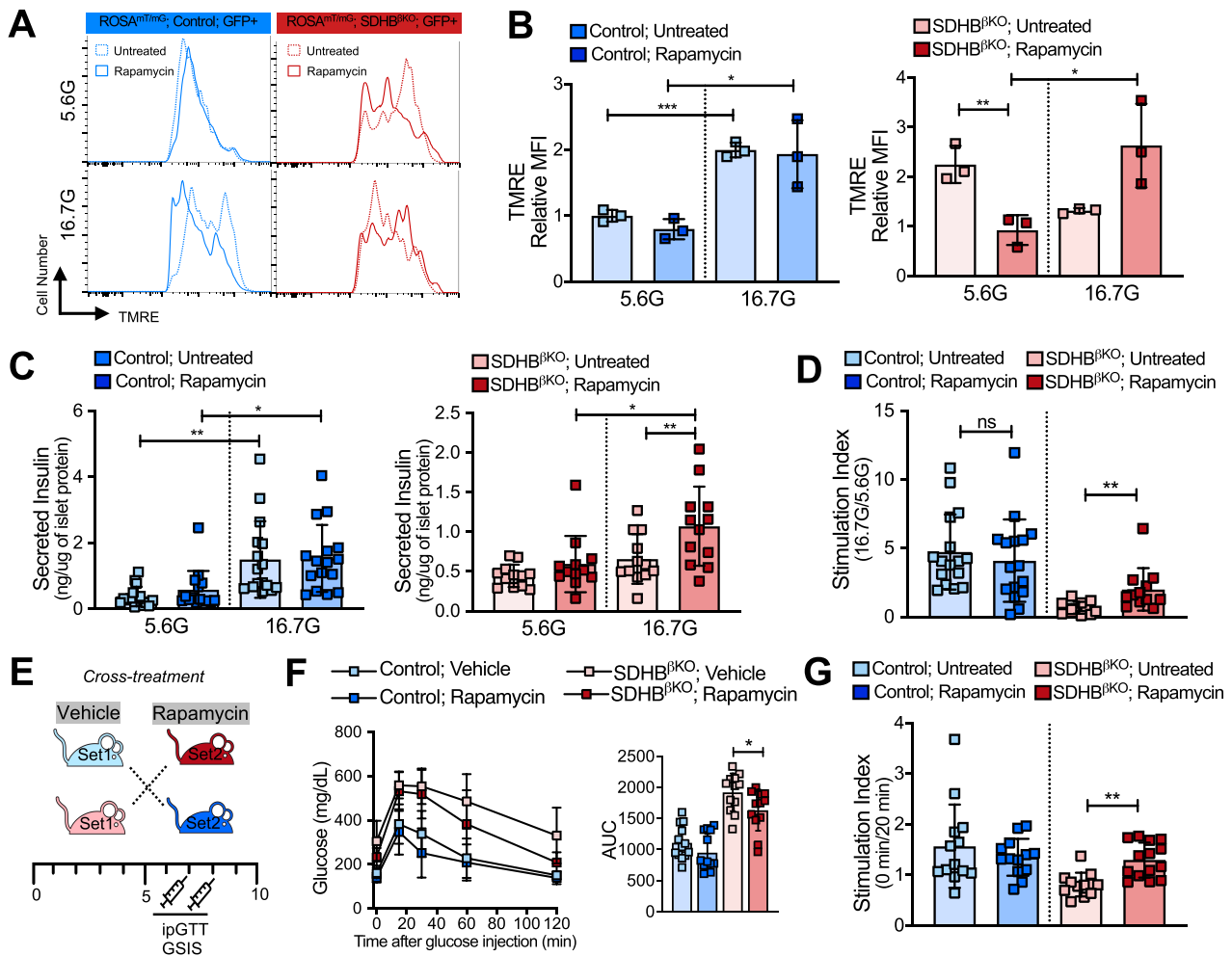
Figure 6—Rapamycin restores mitochondrial function and GSIS coupling in SDHB$^{\beta KO}$ islets and mice. *A*: Representative FACS analyses of mitochondrial membrane potential (TMRE) in GFP$^+$ cells of dispersed islets from 5-week-old ROSA^{mTmG} control and ROSA^{mTmG} SDHB$^{\beta KO}$ following a 24-h vehicle or 50 nmol/L rapamycin treatment and 4-h exposure to 5.6 mmol/L glucose (5.6G) or 16.7 mmol/L glucose (16.7G). *B*: Median fluorescence intensity (MFI) of TMRE relative to control β-cells at 5.6G in islets isolated from 5-week-old control and SDHB$^{\beta KO}$ mice (*n* = 4/group from two independent experiments). *C*: Insulin secretion following serial exposure to 2.8G and 16.7G in islets isolated from 5-week-old control and SDHB$^{\beta KO}$ mice (*n* = 10/group from three independent experiments). *D*: Insulin secretion Stimulation Index (16.7G/2.8G) of islets following vehicle or rapamycin treatment. *E*: Graphical representation of the in vivo crossover experimental design. Control and SDHB$^{\beta KO}$ mice at 7 weeks were treated with vehicle or 5 mg/kg rapamycin for experimentation. One week later, mice were again vehicle or rapamycin treated, but switched treatment groups (control, *n* = 7; SDHB$^{\beta KO}$, *n* = 6). *F*: Intraperitoneal GTT (ipGTT) performed 1 h after injection in control (*n* = 14) and SDHB$^{\beta KO}$ mice (*n* = 12). Corresponding area under the curve (AUC) plot shown at right. *G*: Insulin Stimulation Index (fold-change in insulin secretion at 20 min post–glucose injection relative to 0 min) in mice injected with 5 mg/kg rapamycin or vehicle. Data represented as mean ± SD and were analyzed by two-way ANOVA with Sidak posttest (*B*, *C*, and *F*), unpaired *t* test (AUC plots; *D* and *G*). *$P < 0.05$; **$P < 0.01$; ***$P < 0.001$.

T2D (19,20). Moreover, we observed increased expression of the desuccinylase enzyme SIRT5 in T2D β-cells. This finding implicates *SIRT5* upregulation in T2D (39) as a counterregulatory mechanism for excess protein succinylation that occurs in the context of SDH enzyme dysfunction (23,24). This mechanism was mirrored in SDHB$^{\beta KO}$ mice. Hence, reduced SDH activity is likely to be an underappreciated contributing mechanism to human diabetes (Fig. 7*A*).

SDHB$^{\beta KO}$ mice are a new model of early-onset diabetes caused by β-cell metabolic dysfunction occurring in the absence of dietary and/or obesity-related challenge (peripheral resistance), a phenotype that parallels age-related insulinopenic diabetes (40). A unique aspect of our mouse model, in contrast to mitochondrial diabetes models based upon *Pgc1α* or *Tfam* mutation (41,42), is the prominent impairment of mitochondrial function despite retention of mitochondrial mass and integrity. Interestingly, the
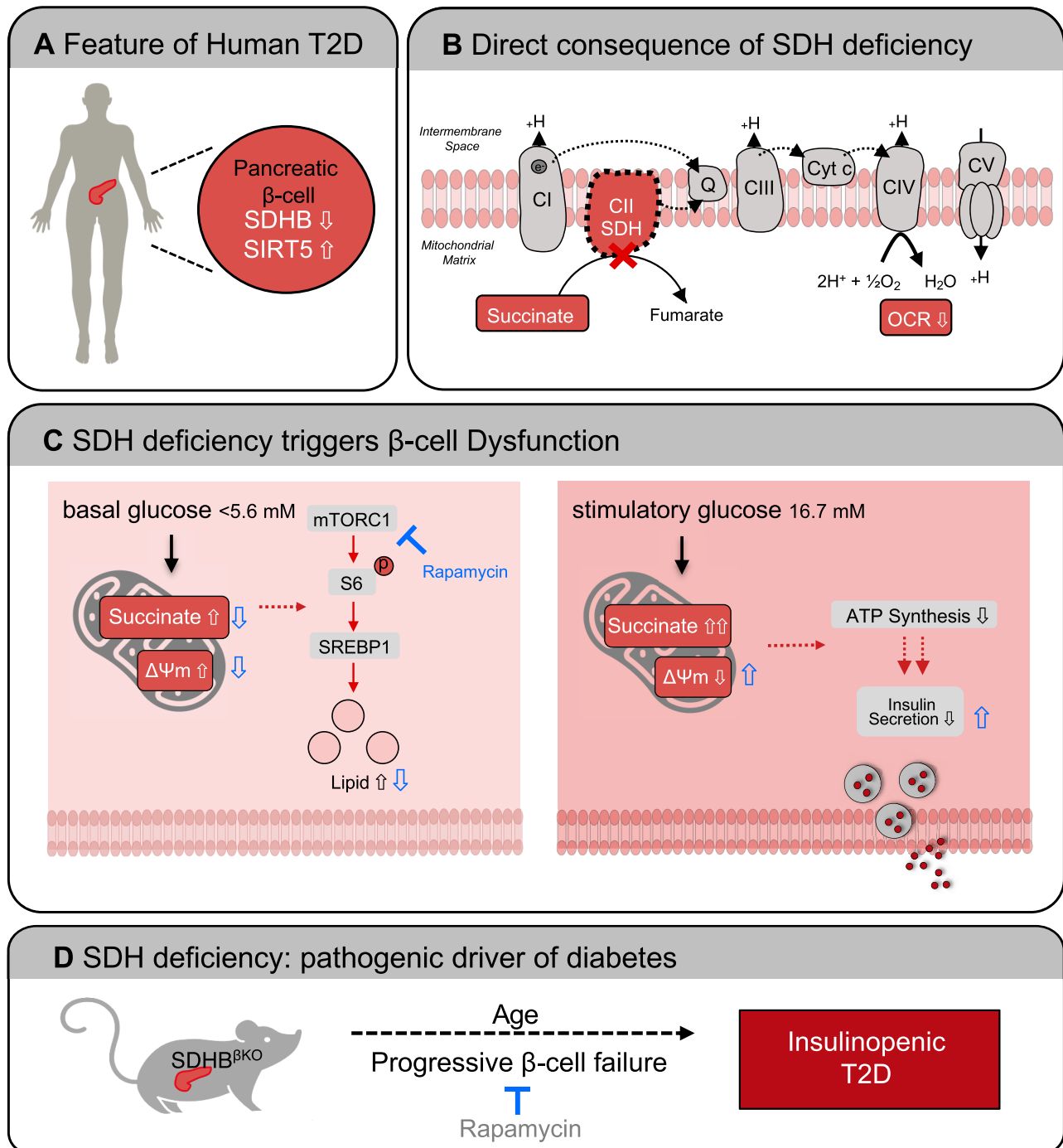
Figure 7—Schematic representation of SDH deficiency–induced insulinopenic T2D. *A*: Reduced SDHB and increased SIRT5 protein expression are features of human T2D. *B*: SDH deficiency directly impairs the OCR and increases succinate accumulation. *C*: Under basal glucose conditions, $\Delta\Psi m$ is hyperpolarized and succinate aberrantly induces mTORC1-regulated lipid synthesis. At stimulatory glucose levels, further increased succinate impairs maintenance of $\Delta\Psi m$ and reduces ATP generation, compromising insulin secretion. Treatment with the mTORC1 inhibitor rapamycin (blue arrows) reduces succinate levels and lowers $\Delta\Psi m$ under basal conditions. Importantly, rapamycin rescues the paradoxical loss of $\Delta\Psi m$ with high glucose exposure and improves GSIS. *D*: Mitochondrial dysfunction (respiratory deficits, compromised bioenergetics, and metabolic alterations) leads to progressive β-cell failure and pubertal-age onset of insulinopenic diabetes in SDHB[βKO] mice. We propose the loss of SDH activity and mTORC1 pathway activation as pathogenic features of diabetes. Consequently, targeted mTORC1 inhibition with rapamycin may be a potential therapeutic strategy for mitochondrial dysfunction–associated β-cell failure. Cyt c, cytochrome c.

metabolic phenotype of SDHB[βKO] mice is both overlapping and distinct from mice with β-cell–targeted disruption of fumarate hydratase (FH1βKO), the TCA cycle enzyme immediately downstream of SDH (43). Similar to SDHB[βKO] mice, FH1βKO mice exhibit a progressive age-dependent diabetes that begins with glucose intolerance at

9–12 weeks of age. However, FH1βKO demonstrated normal glucose-stimulated ATP generation in the prediabetic state that deteriorated in parallel with the development of dysglycemia, indicating an acquired mitochondrial defect. Our extensive characterization of prediabetic SDHB-deficient β-cells revealed defects characteristic of T2D, such as respiratory deficiency (44), compromised bioenergetics (45), and lipid accumulation (6,46) that preceded dysglycemia. Therefore, SDHB$^{\beta KO}$ mice provide a valuable model to study the mitochondrial metabolic phenotype of β-cells in T2D.

The direct consequences of SDH deficiency in β-cell are twofold (Fig. 7B): 1) abrogation of CII activity in the ETC reduces basal mitochondrial respiration (↓OCR); and 2) loss of succinate oxidation to fumarate in the TCA cycle results in excess succinate accumulation (>20-fold ↑). These respiratory and metabolic deficits affect the $\Delta\Psi$m and proton gradient (ΔpH), which are essential for generating the bioenergetic force to synthesize ATP and maintain GSIS (47). In fact, SDHB$^{\beta KO}$ islets demonstrated elevated $\Delta\Psi$m under basal glucose conditions and a paradoxical loss of $\Delta\Psi$m upon glucose exposure (Fig. 7C). $\Delta\Psi$m is established primarily by CI, CIII, and CIV activity, which display intact function in prediabetic SDHB$^{\beta KO}$ islets. Additionally, $\Delta\Psi$m may be increased by high levels of metabolic substrates (32), such as succinate and glycerol phosphate (48) that accumulate in SDHB$^{\beta KO}$ islets (Supplementary Figs. 4A and 6), and mTORC1 hyperactivation (31). Hence, we suspect mitochondrial hyperpolarization of SDHB$^{\beta KO}$ β-cells is due to a combination of reduced basal oxygen consumption, accumulation of intermediary metabolites (including succinate), and mTORC1 hyperactivity. Additionally, the glucose-dependent $\Delta\Psi$m collapse in SDHB$^{\beta KO}$ β-cells is likely a consequence of increased mitochondrial matrix acidification that occurs via excessive glucose-induced succinate accumulation. Succinate is a diprotic acid with similar physiochemical properties to fumarate, which, upon accumulation, acidifies the mitochondrial matrix and reduces $\Delta\Psi$m (43), compromising β-cell mitochondrial bioenergetics and ATP generation. These findings highlight the essential role of SDH/CII activity in maintaining β-cell $\Delta\Psi$m and responding to metabolic demands as well as the detrimental effects of succinate accumulation and mTORC1 hyperactivity (29,30).

A central finding of our study is that prediabetic SDHB$^{\beta KO}$ islets exhibit succinate-dependent mTORC1 hyperactivation. This is supported by increased S6 phosphorylation as well as an mTORC1-dependent transcription and metabolic alterations (enhanced SREBP-regulated lipid synthesis). Although mTORC1 plays a role in the regulation of β-cell proliferation and survival under physiological conditions (49), sustained overactivation of the mTORC1-S6K1 pathway is observed in islets of patients with T2D and diabetic rodent models (50,51) and is deleterious to β-cell function in T2D (33,52). In our study, acute mTORC1 inhibition with rapamycin in vitro and in vivo partially rescued SDHB$^{\beta KO}$ islet secretion, consistent with the beneficial effects of rapamycin treatment in a β-cell–specific mouse model of chronic mTORC1 hyperactivation (β-TSC2$^{-/-}$) (50). The rapamycin-induced reversal of $\Delta\Psi$m loss with glucose exposure in SDHB$^{\beta KO}$ islets suggests that rapamycin may improve β-cell function in part by decreasing succinate levels and restoring normal $\Delta\Psi$m (Fig. 7C) (53). While acknowledging the undesirable effect of subacute/chronic systemic rapamycin treatment (38,49), our data support the potential utility of rapamycin to restore dysregulated mitochondrial function in T2D. Moreover, our findings support mTORC1 inhibition as an alleviating strategy for metabolic disturbances associated with diabetes, highlights the antidiabetogenic effects of rapamycin (54,55) and accentuates the need for β-cell–targeted therapeutic delivery (56).

In summary, we propose SDH deficiency as a pathogenic driver of β-cell metabolic dysregulation and mitochondrial dysfunction. Importantly, we provide a new mechanistic perspective on β-cell dysfunction, suggesting that succinate accumulation induces an inappropriate mTORC1 hyperactivation that can be mitigated by mTORC1 inhibition. Beyond its role in diabetes pathogenesis, the loss of SDH/CII activity may be related to human aging as an age-associated decline in SDHB expression and SDH activity has been observed in human fibroblasts (57), and model organisms demonstrate an indispensable role of SDH in longevity (58). Importantly, our findings provide a testable mechanistic explanation of age-dependent decline in mitochondrial function, insulin secretion (44), and islet lipid accumulation (59). More broadly, our studies suggest that SDH deficiency is relevant to metabolic disorders characterized by mitochondrial dysfunction and mTORC1 hyperactivation.

References

1. Chang-Chen KJ, Mullur R, Bernal-Mizrachi E. Beta-cell failure as a complication of diabetes. Rev Endocr Metab Disord 2008;9:329–343

2. Halban PA, Polonsky KS, Bowden DW, et al. β-cell failure in type 2 diabetes: postulated mechanisms and prospects for prevention and treatment. Diabetes Care 2014;37:1751–1758

3. Brereton MF, Rohm M, Ashcroft FM. β-Cell dysfunction in diabetes: a crisis of identity? Diabetes Obes Metab 2016;18(Suppl. 1):102–109

4. Lowell BB, Shulman GI. Mitochondrial dysfunction and type 2 diabetes. Science 2005;307:384–387

5. Ma ZA, Zhao Z, Turk J. Mitochondrial dysfunction and β-cell failure in type 2 diabetes mellitus. Exp Diabetes Res 2012;2012:703538

6. Haythorne E, Rohm M, van de Bunt M, et al. Diabetes causes marked inhibition of mitochondrial metabolism in pancreatic β-cells. Nat Commun 2019;10:2474

7. Wollheim CB, Maechler P. Beta-cell mitochondria and insulin secretion: messenger role of nucleotides and metabolites. Diabetes 2002;51(Suppl. 1):S37–S42

8. Van Vranken JG, Na U, Winge DR, Rutter J. Protein-mediated assembly of succinate dehydrogenase and its cofactors. Crit Rev Biochem Mol Biol 2015;50:168–180

9. Sun F, Huo X, Zhai Y, et al. Crystal structure of mitochondrial respiratory membrane protein complex II. Cell 2005;121:1043–1057

10. Rustin P, Munnich A, Rötig A. Succinate dehydrogenase and human diseases: new insights into a well-known enzyme. Eur J Hum Genet 2002;10:289–291

11. Rutter J, Winge DR, Schiffman JD. Succinate dehydrogenase - Assembly, regulation and role in human disease. Mitochondrion 2010;10:393–401

12. Armstrong N, Storey CM, Noll SE, et al. SDHB knockout and succinate accumulation are insufficient for tumorigenesis but dual SDHB/NF1 loss yields SDHx-like pheochromocytomas. Cell Rep 2022;38:110453

13. Edalat A, Schulte-Mecklenbeck P, Bauer C, et al. Mitochondrial succinate dehydrogenase is involved in stimulus-secretion coupling and endogenous ROS formation in murine beta cells. Diabetologia 2015;58:1532–1541

14. Leibowitz G, Khaldi MZ, Shauer A, et al. Mitochondrial regulation of insulin production in rat pancreatic islets. Diabetologia 2005;48:1549–1559

15. Wojtovich AP, Smith CO, Haynes CM, Nehrke KW, Brookes PS. Physiological consequences of complex II inhibition for aging, disease, and the mKATP channel. Biochim Biophys Acta 2013;1827:598–611

16. Salabei JK, Gibb AA, Hill BG. Comprehensive measurement of respiratory activity in permeabilized cells using extracellular flux analysis. Nat Protoc 2014;9:421–438

17. Navarro G, Abdolazimi Y, Zhao Z, et al. Genetic disruption of adenosine kinase in mouse pancreatic β-cells protects against high-fat diet-induced glucose intolerance. Diabetes 2017;66:1928–1938

18. Abdolazimi Y, Zhao Z, Lee S, et al. CC-401 promotes β-cell replication via pleiotropic consequences of DYRK1A/B inhibition. Endocrinology 2018;159:3143–3157

19. Mootha VK, Lindgren CM, Eriksson KF, et al. PGC-1alpha-responsive genes involved in oxidative phosphorylation are coordinately downregulated in human diabetes. Nat Genet 2003;34:267–273

20. He J, Watkins S, Kelley DE. Skeletal muscle lipid content and oxidative enzyme activity in relation to muscle fiber type in type 2 diabetes and obesity. Diabetes 2001;50:817–823

21. Lashin OM, Szweda PA, Szweda LI, Romani AM. Decreased complex II respiration and HNE-modified SDH subunit in diabetic heart. Free Radic Biol Med 2006;40:886–896

22. El Ouaamari A, Zhou JY, Liew CW, et al. Compensatory islet response to insulin resistance revealed by quantitative proteomics. J Proteome Res 2015;14:3111–3122

23. Smestad J, Erber L, Chen Y, Maher LJ 3rd. Chromatin succinylation correlates with active gene expression and is perturbed by defective TCA cycle metabolism. iScience 2018;2:63–75

24. Rardin MJ, He W, Nishida Y, et al. SIRT5 regulates the mitochondrial lysine succinylome and metabolic networks. Cell Metab 2013;18:920–933

25. Li F, He X, Ye D, et al. NADP(+)-IDH mutations promote hypersuccinylation that impairs mitochondria respiration and induces apoptosis resistance. Mol Cell 2015;60:661–675

26. Weir GC, Bonner-Weir S. Islet β cell mass in diabetes and how it relates to function, birth, and death. Ann N Y Acad Sci 2013;1281:92–105

27. Chen C, Cohrs CM, Stertmann J, Bozsak R, Speier S. Human beta cell mass and function in diabetes: recent advances in knowledge and technologies to understand disease pathogenesis. Mol Metab 2017;6:943–957

28. Marchetti P, Bugliani M, De Tata V, Suleiman M, Marselli L. Pancreatic beta cell identity in humans and the role of type 2 diabetes. Front Cell Dev Biol 2017;5:55

29. Pfleger J, He M, Abdellatif M. Mitochondrial complex II is a source of the reserve respiratory capacity that is regulated by metabolic sensors and promotes cell survival. Cell Death Dis 2015;6:e1835

30. Hawkins BJ, Levin MD, Doonan PJ, et al. Mitochondrial complex II prevents hypoxic but not calcium- and proapoptotic Bcl-2 protein-induced mitochondrial membrane potential loss. J Biol Chem 2010;285:26494–26505

31. Sukumar M, Liu J, Mehta GU, et al. Mitochondrial membrane potential identifies cells with enhanced stemness for cellular therapy. Cell Metab 2016;23:63–76

32. Liesa M, Shirihai OS. Mitochondrial dynamics in the regulation of nutrient utilization and energy expenditure. Cell Metab 2013;17:491–506

33. Vernier S, Chiu A, Schober J, et al. β-cell metabolic alterations under chronic nutrient overload in rat and human islets. Islets 2012;4:379–392

34. Oudijk L, Papathomas T, de Krijger R, et al. The mTORC1 complex is significantly overactivated in SDHX-mutated paragangliomas. Neuroendocrinology 2017;105:384–393

35. Laplante M, Sabatini DM. mTOR signaling in growth control and disease. Cell 2012;149:274–293

36. Saxton RA, Sabatini DM. mTOR signaling in growth, metabolism, and disease. Cell 2017;168:960–976

37. Villa-Cuesta E, Holmbeck MA, Rand DM. Rapamycin increases mitochondrial efficiency by mtDNA-dependent reprogramming of mitochondrial metabolism in Drosophila. J Cell Sci 2014;127:2282–2290

38. Blagosklonny MV. Fasting and rapamycin: diabetes versus benevolent glucose intolerance. Cell Death Dis 2019;10:607

39. Ma Y, Fei X. SIRT5 regulates pancreatic β-cell proliferation and insulin secretion in type 2 diabetes. Exp Ther Med 2018;16:1417–1425

40. Stidsen JV, Henriksen JE, Olsen MH, et al. Pathophysiology-based phenotyping in type 2 diabetes: a clinical classification tool. Diabetes Metab Res Rev 2018;34:e3005

41. Silva JP, Köhler M, Graff C, et al. Impaired insulin secretion and beta-cell loss in tissue-specific knockout mice with mitochondrial diabetes. Nat Genet 2000;26:336–340

42. Rowe GC, Arany Z. Genetic models of PGC-1 and glucose metabolism and homeostasis. Rev Endocr Metab Disord 2014;15:21–29

43. Adam J, Ramracheya R, Chibalina MV, et al. Fumarate hydratase deletion in pancreatic β cells leads to progressive diabetes. Cell Rep 2017;20:3135–3148

44. Gregg T, Poudel C, Schmidt BA, et al. Pancreatic β-cells from mice offset age-associated mitochondrial deficiency with reduced KATP channel activity. Diabetes 2016;65:2700–2710

45. Wikstrom JD, Sereda SB, Stiles L, et al. A novel high-throughput assay for islet respiration reveals uncoupling of rodent and human islets. PLoS One 2012;7:e33023

46. Oh YS, Bae GD, Baek DJ, Park EY, Jun HS. Fatty acid-induced lipotoxicity in pancreatic beta-cells during development of type 2 diabetes. Front Endocrinol (Lausanne) 2018;9:384

47. Gerencser AA. Metabolic activation-driven mitochondrial hyperpolarization predicts insulin secretion in human pancreatic beta-cells. Biochim Biophys Acta Bioenerg 2018;1859:817–828

48. van Raam BJ, Sluiter W, de Wit E, Roos D, Verhoeven AJ, Kuijpers TW. Mitochondrial membrane potential in human neutrophils is maintained by complex III activity in the absence of supercomplex organisation. PLoS One 2008;3:e2013

49. Ardestani A, Lupse B, Kido Y, Leibowitz G, Maedler K. mTORC1 signaling: a double-edged sword in diabetic β cells. Cell Metab 2018;27:314–331

50. Bartolomé A, Kimura-Koyanagi M, Asahara S, et al. Pancreatic β-cell failure mediated by mTORC1 hyperactivity and autophagic impairment. Diabetes 2014;63:2996–3008

51. Yuan T, Rafizadeh S, Gorrepati KD, et al. Reciprocal regulation of mTOR complexes in pancreatic islets from humans with type 2 diabetes. Diabetologia 2017;60:668–678

52. Bachar E, Ariav Y, Ketzinel-Gilad M, Cerasi E, Kaiser N, Leibowitz G. Glucose amplifies fatty acid-induced endoplasmic reticulum stress in pancreatic beta-cells via activation of mTORC1. PLoS One 2009;4:e4954

53. Dou X, Sun Y, Li J, et al. Short-term rapamycin treatment increases ovarian lifespan in young and middle-aged female mice. Aging Cell 2017;16:825–836

54. Andreux PA, Houtkooper RH, Auwerx J. Pharmacological approaches to restore mitochondrial function. Nat Rev Drug Discov 2013;12:465–483

55. Reifsnyder PC, Flurkey K, Te A, Harrison DE. Rapamycin treatment benefits glucose metabolism in mouse models of type 2 diabetes. Aging (Albany NY) 2016;8:3120–3130

56. Horton TM, Allegretti PA, Lee S, Moeller HP, Smith M, Annes JP. Zinc-chelating small molecules preferentially accumulate and function within pancreatic β cells. Cell Chem Biol 2019;26:213–222.e6

57. Bowman A, Birch-Machin MA. Age-dependent decrease of mitochondrial complex II activity in human skin fibroblasts. J Invest Dermatol 2016;136:912–919

58. Walker DW, Hájek P, Muffat J, et al. Hypersensitivity to oxygen and shortened lifespan in a Drosophila mitochondrial complex II mutant. Proc Natl Acad Sci USA 2006;103:16382–16387

59. Tong X, Dai C, Walker JT, et al. Lipid droplet accumulation in human pancreatic islets is dependent on both donor age and health. Diabetes 2020;69:342–354